

Design of new Mott multiferroics via complete charge transfer: promising candidates for bulk photovoltaics

Hanghui Chen^{1,2*} and Andrew Millis³

¹*NYU-ECNU Institute of Physics,
NYU Shanghai, Shanghai 200062, China*

²*Department of Physics,
New York University,
New York, NY 10002, USA*

³*Department of Physics,
Columbia University,
New York, NY, 10027, USA*

(Dated: July 25, 2018)

Abstract

Optimal materials to induce bulk photovoltaic effects should lack inversion symmetry and have an optical gap matching the energies of visible radiation. Ferroelectric perovskite oxides such as BaTiO₃ and PbTiO₃ exhibit substantial polarization and stability, but have the disadvantage of excessively large band gaps. We use both density functional theory and dynamical mean field theory calculations to design a new class of Mott multiferroics—double perovskite oxides A_2VFeO_6 (A =Ba, Pb, etc). While neither perovskite AVO_3 nor $AFeO_3$ is ferroelectric, in the double perovskite A_2VFeO_6 a ‘complete’ charge transfer from V to Fe leads to a non-bulk-like charge configuration—an empty V- d shell and a half-filled Fe- d shell, giving rise to a polarization comparable to that of ferroelectric ATiO₃. Different from nonmagnetic ATiO₃, the new double perovskite oxides have an antiferromagnetic ground state and around room temperatures, are paramagnetic Mott insulators. Most importantly, the V d^0 state significantly reduces the band gap of A_2VFeO_6 , making it smaller than that of ATiO₃ and BiFeO₃ and rendering the new multiferroics a promising candidate to induce bulk photovoltaic effects.

* Correspondence to hanghui.chen@nyu.edu

I. INTRODUCTION

The lack of inversion symmetry caused by ferroelectric ordering in certain transition metal oxides can separate the electrons and holes generated by photo-excitation, making these materials promising candidates for photovoltaic devices [1–4]. However, many known ferroelectric perovskite oxides including BaTiO_3 and PbTiO_3 have very large band gaps ($\sim 3\text{--}5$ eV) [5], significantly limiting their absorption efficiency in the visible frequency range. The large band gap is intrinsic: it is set by the energy difference between the Ti- d and O- p levels, which is large because Ti and O have substantially different electronegativity. Intensive research in perovskite oxides has focused on reducing band gaps while maintaining ferroelectric polarization. One approach is to replace a fraction of transition metal ions with a different cation; with one transition metal species driving ferroelectricity and the other providing lower energy states that reduce the band gap [6–11]. Using this approach, band gap reductions by ~ 1 eV have been attained [10] and a high power conversion efficiency has been experimentally achieved in $\text{Bi}_2\text{FeCrO}_6$ [11]. In another method, a class of layered double perovskite oxides $AA'BB'O_6$ has been theoretically proposed, in which a large in-plane polarization is found via nominal d^0 filling on the B -site, A -site cations bearing lone-pair electrons, and $A' \neq A$ size mismatch; the band gap is controlled by B/B' electronegativity difference [12].

In this work, we propose a simple design scheme. We introduce a new class of double perovskite oxides $A_2\text{VFeO}_6$ where A is a divalent cation ($A=\text{Ba}, \text{Pb}$, etc) and demonstrate that a ‘complete’ charge transfer (nominally one electron transfer) between the two transition metal ions [13–18] can induce desirable properties for bulk photovoltaics. First-principles calculations show that while neither bulk perovskite AVO_3 nor AFeO_3 is ferroelectric, a ‘complete’ charge transfer occurs from V to Fe, rendering the new double perovskite oxides a Mott multiferroic: at zero temperature a ferroelectric antiferromagnet and around room temperatures a ferroelectric Mott insulator. The ferroelectric polarization is substantial, comparable to ATiO_3 , but the band gap is significantly lower, smaller than that of ATiO_3 and BiFeO_3 .

We first focus on Ba_2VFeO_6 (similar results are obtained for Pb_2VFeO_6 and Sr_2VFeO_6 , see section IV). Fig. 1a and b show the atomic and electronic structures for perovskite BaVO_3 and BaFeO_3 , respectively. Bulk perovskite BaVO_3 has been recently synthesized at high

pressure and has been found to remain cubic and metallic to the lowest temperature [19]. Bulk BaFeO_3 normally crystallizes in a hexagonal structure but cubic perovskite BaFeO_3 can be stabilized in powders [20] and in epitaxial thin films [21–24] and exhibits a robust ferromagnetism [20–24]. Both metallic [20, 23] and insulating [21, 22, 24] behaviors have been reported.

Formal valence considerations imply that in BaVO_3 the V adopts a d^1 configuration while in BaFeO_3 the Fe is d^4 . In the double perovskite Ba_2VFeO_6 , however, we expect that the large electronegativity difference between V and Fe leads to complete charge transfer from V to Fe, resulting in $\text{V-}d^0$ and $\text{Fe-}d^5$ configurations as illustrated in Fig. 1c. Similar phenomena have been predicted and observed in many different transition metal oxide heterostructures [15–18, 25]. The particular relevance here is that the empty V- d shell and half-filled Fe- d shell are both susceptible to noncentrosymmetric distortions (for the empty d shell case, see [26, 27] and for the half-filled d shell cases see [28–30]) while $\text{Ba}^{2+}\text{-O}^{2-}$ coupling stabilizes the ferroelectric phase over anti-ferroelectric phases, as in BaTiO_3 [31]. The half filled Fe- d shell leads to magnetic ordering and Mott insulating behavior, while the position of the V- d level leads to a reduced band gap (a similar strategy to reduce band gap has been discussed in Refs. [12, 26, 27]. Therefore as Fig. 1c shows, double perovskite Ba_2VFeO_6 is predicted to be Mott multiferroic (paramagnetic ferroelectric at high temperatures and long-range magnetically ordered at sufficiently low temperatures). Furthermore, as illustrated in Fig. 1c, the band gap of double perovskite Ba_2VFeO_6 is set by the filled lower Hubbard band of Fe- d states (strongly hybridized with O- p states) and empty V- d states (conduction band edge).

We note that the double perovskite structure is much more stable than the layered configuration as proposed in Ref. [12], because charge transfer generically results in substantial metal-oxygen bond disproportionation [25]. Due to geometry consideration, the bond disproportionation inevitably induces internal strain in the layered structure but is naturally accommodated by the double perovskite structure, which explains the phase stability [25]. Also different from previous speculation that rock-salt ordering of B -site atoms suppress polarization in $A_2BB'\text{O}_6$ [12, 32], our work shows that it is possible to induce robust ferroelectricity in double perovskite oxides Ba_2VFeO_6 .

In the rest of this paper we present calculations substantiating this picture. In Section II we outline the computational details. In Section III we present results for double perovskite

Ba₂VFeO₆. Section IV extends the calculations to the double perovskite Pb₂VFeO₆ and Sr₂VFeO₆, in which we discuss the similarities and differences. Section V is a summary and conclusion.

II. COMPUTATIONAL DETAILS

Our first-principles calculations are performed using density functional theory (DFT) [33] and dynamical mean field theory (DMFT) [34]. Structural relaxation is performed within DFT. Gaps are calculated using both DFT and DFT+DMFT. It is known in literature that structural and magnetic properties of multiferroic oxides strongly depend on the choice of exchange correlation functionals [5, 30, 35]. We use three exchange correlation functionals to test the robustness of our predictions: i) charge-density-only generalized gradient approximation with Perdew-Burke-Ernzerhof parametrization [36] plus Hubbard U and Hund's J corrections (PBE+ U + J) [37], ii) charge-only local density approximation with Hubbard U and Hund's J corrections (LDA+ U + J) [37, 38]; iii) spin-polarized generalized gradient approximation with Perdew-Burke-Ernzerhof parametrization revised for solids (sPBEsol) [39]. In order to investigate Mottness and effects of long-range magnetic ordering, we use DMFT to study both paramagnetic and long-range magnetic ordered states.

The DFT calculations are performed using a plane-wave basis [33], as implemented in the Vienna Ab-initio Simulation Package (VASP) [40, 41]. The Projector Augmented Wave (PAW) approach is used [42, 43]. We use an energy cutoff of 600 eV. All the supercells of double perovskite oxides A_2 VFeO₆ consist of 40 atoms to accommodate different magnetic orderings. We consider ferromagnetic ordering, [001] antiferromagnetic ordering, [010] antiferromagnetic ordering and [100] antiferromagnetic ordering (see the Supplementary Materials for their definitions). A $6 \times 6 \times 6$ Monkhorst-Pack grid is used to sample the Brillouin zone. Both cell and internal coordinates are fully relaxed until each force component is smaller than 10 meV/Å and the stress tensor is smaller than 0.1 kbar.

In the PBE+ U + J /LDA+ U + J as well as DMFT calculations, we use $U_{\text{Fe}} = 5$ eV, $J_{\text{V}} = J_{\text{Fe}} = 0.7$ eV, following previous studies [44, 45]. The choice of U_{V} needs caution. While U_{V} of about 5 eV has been accepted in literature [44], we find that $U_{\text{V}} = 5$ eV induces off-center displacement δ_{VO} in perovskite BaVO₃, while in experiment the perovskite BaVO₃ is stabilized in a cubic structure under 15 GPa [19]. The off-center displacement of V is closely

related to orbital ordering ($d_{xy}^1 d_{xz}^0 d_{yz}^0$) stabilized by a large U_V in the DFT+ U method. Therefore we use a smaller $U_V = 3$ eV which stabilizes a cubic structure in perovskite BaVO_3 to calculate double perovskite oxides Ba_2VFeO_6 . This ensures that a non-zero δ_{VO} in Ba_2VFeO_6 is not a consequence of a large U_V , but rather is induced by charge transfer. We repeat all the DFT calculations on Ba_2VFeO_6 using $U_V = 5$ eV and find qualitatively similar results in structural properties. On the other hand, U_V controls the energy level of V- d states, which may affect the band gap of Ba_2VFeO_6 . Therefore, in our DMFT calculations, we also study a range of U_V (from 3 to 6 eV) to estimate the variation of energy gap in the spectral function.

We perform single-site DMFT calculations with Ising-like Slater-Kanamori interactions. The impurity problem is solved using the continuous-time quantum Monte Carlo algorithm with a hybridization expansion [46, 47]. The correlated subspace and the orbitals with which it mixes are constructed using maximally localized Wannier functions [48] defined over the full 10 eV range spanned by the p - d band complex, resulting in a well-localized set of d -like orbitals. All the DMFT calculations are performed at the temperature of 290 K. For each DMFT iteration, a total of 3.8 billion Monte Carlo steps is taken to converge the impurity Green function and self energy. In double perovskite oxides, since V- d states are empty, we treat V- t_{2g} orbitals with the DMFT method and V- e_g orbitals with a static Hartree-Fock approximation. Because Fe- d states are half-filled, we treat all the five Fe- d orbitals with the DMFT method. The two self energies (one for V sites and the other for Fe sites) are solved independently and then coupled at the level of self-consistent conditions.

To obtain the spectral functions, the imaginary axis self energy is continued to the real axis using the maximum entropy method [49]. Then the real axis local Green function is calculated using the Dyson equation and the spectral function is obtained following:

$$A_i(\omega) = -\frac{1}{\pi} \text{Im} G_i^{\text{loc}}(\omega) = -\frac{1}{\pi} \text{Im} \left(\sum_{\mathbf{k}} \frac{1}{(\omega + \mu) \mathbf{1} - H_0(\mathbf{k}) - \Sigma(\omega)} \right)_{ii} \quad (1)$$

where i is the label of a Wannier function. $\mathbf{1}$ is an identity matrix, $H_0(\mathbf{k})$ is the DFT-PBE band Hamiltonian in the matrix form using the Wannier basis. $\Sigma(\omega)$ is understood as a diagonal matrix only with nonzero entries on the correlated orbitals. μ is the chemical potential. V_{dc} is the fully localized limit (FLL) double counting potential, which is defined as [50]:

$$V_{dc} = (U - 2J) \left(N_d - \frac{1}{2} \right) - \frac{1}{2} J(N_d - 3) \quad (2)$$

where N_d is the d occupancy of a correlated site.

III. RESULTS OF Ba_2VFeO_6

A. Structural properties

We first discuss the fully relaxed atomic structure of double perovskite Ba_2VFeO_6 , obtained using DFT calculations with three different exchange correlation functionals (PBE+ U + J , LDA+ U + J and sPBEsol). For each exchange correlation functional, we test ferromagnetic (F), [001] antiferromagnetic, [010] antiferromagnetic and [100] antiferromagnetic orderings (see the Supplementary Materials for precise definitions). For each case, we start from a crystal structure with rotations and tilts of VO_6 and FeO_6 (space group $P2_1/n$) and then perturb the V and Fe atoms along [001] or (011) and (111) directions. Next we perform atomic relaxation with all the symmetry turned off. After atomic relaxation, we find that the rotations and tilts of VO_6 and FeO_6 are strongly suppressed while the polarization along [001] or (011) or (111) direction is stabilized. Comparing the total energy between three polarizations, we find the ground state of Ba_2VFeO_6 has the polarization along the [001] direction. The ground state structure has tetragonal symmetry (space group $I4/m$). On the magnetic properties, given the U and J values, we find that the ground state is always of the [001] antiferromagnetic ordering. Using the same methods and parameters, perovskite BaVO_3 and BaFeO_3 have cubic symmetry. The resulting lattice constant a , tetragonality c/a ratio and cation-displacement δ_{BO} along the [001] direction (see in Fig. 1c) are shown in Table I for each exchange correlation functional. The full crystal structure data are provided in the Supplementary Materials. We need to point out that the reason that rotations and tilts of VO_6/FeO_6 octahedra are strongly suppressed in Ba_2VFeO_6 is due to the large ionic size of Ba ions, which is known to prohibit rotations and tilts of oxygen octahedra in perovskite Ba-compounds and to induce robust ferroelectricity in BaTiO_3 and BaMnO_3 [29, 51].

For comparison, we also calculate the atomic structure of fully relaxed tetragonal BaTiO_3 , a known ferroelectric perovskite. Since BaTiO_3 is a d^0 band insulator with no magnetic prop-

erties, we do not add Hubbard U and Hund's J correction to PBE/LDA and we use PBEsol instead of spin-polarized PBEsol (sPBEsol). We find that the calculated c/a ratio and ion-displacement (δ_{VO} and δ_{FeO}) of Ba_2VFeO_6 are comparable to those of BaTiO_3 . The ground state of tetragonal double perovskite Ba_2VFeO_6 is an insulator (we will discuss the gap properties in details in the following subsections). The ground state of high-symmetry cubic double perovskite Ba_2VFeO_6 is also an insulator (see Table I). Therefore a switching path for ferroelectric polarization is well-defined and we can use the Berry phase method [48] to calculate the polarization of the tetragonal structure. We find that for each exchange-correlation function the calculated polarization of Ba_2VFeO_6 is comparable to that of BaTiO_3 (see Table I).

We comment here that our recent study [30, 35] of perovskite manganites show that PBE+ $U+J$ and sPBEsol yield the most accurate predictions on structural and magnetic properties of magnetic ferroelectrics, while LDA+ $U+J$ sets an conservative estimation for the lower bound of polarization. Therefore we believe that the polarization of Ba_2VFeO_6 is larger than $18 \mu\text{C}/\text{cm}^2$, which is substantial enough to induce bulk photovoltaic effects [4].

B. Electronic properties

The results of the previous subsection indicate that the double perovskite Ba_2VFeO_6 has a noncentrosymmetric tetragonal distortion not found in the component materials bulk BaVO_3 and BaFeO_3 . In this section we consider the electronic reconstruction arising in the double perovskite.

Fig. 2a shows the band structure of double perovskite Ba_2VFeO_6 with the [001] antiferromagnetic ordering (only one spin channel is shown here), calculated using the PBE+ $U+J$ method. We see that a gap is clearly opened in Ba_2VFeO_6 while using the same method with the same parameters, perovskite BaVO_3 and BaFeO_3 are found to be metallic with V- d and Fe- d states at the Fermi surface (see Section II in the Supplementary Materials for details). The gap opening in Ba_2VFeO_6 is a strong evidence of a nominally “complete” charge transfer from V to Fe. A similar charge-transfer-driven metal-insulator transition is predicted [52] and observed [17] in $\text{LaTiO}_3/\text{LaNiO}_3$ superlattices.

For comparison, we also calculate the band structure of tetragonal BaTiO_3 using PBE (Fig. 2b). We note that while the polarization of double perovskite Ba_2VFeO_6 is comparable

to that of BaTiO₃, the band gap of Ba₂VFeO₆ (0.78 eV) is significantly smaller than that of BaTiO₃ (1.75 eV). Using other exchange correlation functionals, we find similar properties that the band gap of Ba₂VFeO₆ is smaller than that of BaTiO₃ by about 1 eV (see ‘fundamental gap’ Δ_0 in Table I).

For photovoltaic effects the relevant quantity is the optical gap Δ_{optical} . We calculate the optical conductivity of both Ba₂VFeO₆ and BaTiO₃ using standard methods [53] and show the results in Fig. 2c. Due to the tetragonal symmetry, the off-diagonal matrix elements of the optical conductivity vanish and only two diagonal elements are independent ($\sigma_{xx} = \sigma_{yy}$ and σ_{zz}). For BaTiO₃ the minimum optical gap is in the xx channel and is given by the direct (vertical in momentum space) gap (shown for BaTiO₃ as the blue arrow in Fig. 2b). In BaTiO₃ the optical gap is larger than the fundamental gap, which is indirect (momentum of lowest conduction band state differs from momentum of highest valence band state; the green arrow in Fig. 2c shows the size of the fundamental gap). The optical conductivity of Ba₂VFeO₆ is also larger than its fundamental gap, which can be understood in a similar manner. If we consider (VFe) as a pseudo-atom X , the hypothetical single perovskite BaXO₃ would have an indirect gap (between Γ and R). However, the reduction in translational symmetry due to the V-Fe alternation leads to band folding which maps the original R point to the Γ point, leading to a direct gap of 0.8 eV at the Γ point. However the calculated optical gap is 1.1 eV (blue arrow in Fig. 2a). The difference between the direct and optical gaps is a matrix element effect: the lowest back-folded conduction band state does not have a dipole allowed transition matrix element with the highest-lying valence band state (see the Supplementary Materials for more details).

It is well-known that DFT with semi-local exchange correlation functionals substantially underestimate band gaps. Here we argue that since Ba₂VFeO₆ and BaTiO₃ have similar electronic structures (gap separated by metal d and oxygen p states), the DFT band gap underestimation with respect to experimental values is approximately a constant for BaTiO₃ and Ba₂VFeO₆. The experimental optical gap of BaTiO₃ is 3.2 eV and the DFT calculated value is 2.3 eV, about 0.9 eV smaller. The DFT calculated optical gap of Ba₂VFeO₆ is 1.1 eV, hence we estimate the experimental optical gap of Ba₂VFeO₆ is 2.0 eV, which is smaller than the optical gap of intensively investigated BiFeO₃ (2.7 eV) [54].

We comment here that while we use the assumption that our DFT band gap underestimation (0.9 eV) applies to both BaTiO₃ and Ba₂VFeO₆, our results that Ba₂VFeO₆ should

have a smaller gap than that of BaTiO_3 and BiFeO_3 are supported by physical arguments (see Fig. 3). The band gap for transition metal oxides is set by the energy difference between transition metal d states and oxygen p states. This p - d separation is a measure of the relative electronegativity of transition metal and oxygen ions. Ti and V are both first-row transition metals and in BaTiO_3 and Ba_2VFeO_6 , Ti and V both have a d^0 configuration. Because V has a larger nuclear charge than Ti, the V- d states have lower energies than the Ti- d states, which leads to a smaller band gap for Ba_2VFeO_6 than for BaTiO_3 (compare panels **a** and **c** of Fig. 3). On the other hand, the Fe d states are half-filled in both Ba_2VFeO_6 and BiFeO_3 , while V- d states are empty in Ba_2VFeO_6 . Due to Coulomb repulsion and Hund's coupling effects, adding one more electron in a half-filled d shell generically costs more energy than adding an electron in an empty d shell. Therefore the upper Hubbard band of Fe d states have higher energy than V d states, which results in a larger band gap for BiFeO_3 than for Ba_2VFeO_6 (compare panels **b** and **c** of Fig. 3).

C. Estimation of critical temperatures

Double perovskite Ba_2VFeO_6 is a type-I multiferroic [55], in which ferroelectric polarization and magnetism arise from different origins and they are largely independent of one another. This means that ferroelectric polarization and magnetism have their own critical temperatures and usually the critical temperature of polarization (T_C) is higher than the critical temperature of magnetism (T_N) [56]. In this subsection, we estimate T_C and T_N for Ba_2VFeO_6 .

Estimation of T_C : in order to estimate the ferroelectric Curie temperature T_C , we use the predictor $T_C \propto P_0^2$ where P_0 is the zero-temperature polarization [57]. This predictor has been successfully applied to a wide range of Pb-based perovskite ferroelectric oxides and it yields an accurate and quantitative estimation for ferroelectric T_C [58]. We apply this predictor to our Ba-based ferroelectrics, i.e. BaTiO_3 and Ba_2VFeO_6 . Here we use tetragonal BaTiO_3 as the reference system. The experimental Curie temperature T_C for BaTiO_3 is about 400 K [59]. Using the DFT+Berry phase method [48], we can obtain the values of the zero-temperature polarization for both BaTiO_3 and Ba_2VFeO_6 shown in Table I. Therefore we estimate that T_C for Ba_2VFeO_6 is 473 K (PBE+ U + J), 245 K (LDA+ U + J) and 425 K (sPBEsol). While different exchange correlation functionals predict a range for T_C , we find

that T_C is near or above room temperature.

Estimation of T_N : we use a classical Heisenberg model $E = \frac{1}{2} \sum_{\langle kl \rangle} J_{kl} \mathbf{S}_k \cdot \mathbf{S}_l$ to estimate the magnetic ordering transition temperature T_N , where \mathbf{S}_k is a unit-length classical spin and $\langle kl \rangle$ denotes summation over nearest Fe neighbors. Here we only consider Fe-Fe exchange couplings. Because double perovskite Ba_2VFeO_6 has a tetragonal structure, there are two exchange couplings of J_{kl} : J_{in} for the short Fe-Fe bonds and J_{out} for the long Fe-Fe bonds. By calculating the total energy for the ferromagnetic ordering, [001] antiferromagnetic ordering and [100] antiferromagnetic ordering, we obtain that the in-plane exchange coupling J_{in} is 2.5 meV (PBE+ $U+J$), 3.7 meV (LDA+ $U+J$) and 3.1 meV (sPBEsol); and the out-of-plane exchange coupling J_{out} is 3.1 meV (PBE+ $U+J$), 4.0 meV (LDA+ $U+J$) and 3.7 meV (sPBEsol). The positive sign means that exchange couplings are all antiferromagnetic. Based on a mean-field theory, the estimated Néel temperature is $T_N = |4J_{\text{in}} - 8J_{\text{out}}|$. The minus sign is because on a quasi face-centered-cubic lattice, every Fe atom has 8 nearest neighbors that are antiferromagnetically coupled and 4 nearest neighbors that are ferromagnetically coupled. Therefore T_N is estimated to be 172 K (PBE+ $U+J$), 200 K (LDA+ $U+J$) and 200 K (sPBEsol). Since mean-field theories usually overestimate magnetic transition temperatures, the actual T_N could be lower. An experimental determination of the magnetic ordering temperature would be of great interest.

D. Effects of long-range orders

The estimates for the ferroelectric and magnetic transition temperatures of Ba_2VFeO_6 suggest that its actual ferroelectric Curie temperature T_C is probably higher than its actual Néel temperature T_N , as is the case for most type-I multiferroics [55]. It is therefore important to ask if the magnetically disordered state remains insulating, so that the ferroelectric properties are preserved.

Here we use DFT+DMFT to study both the paramagnetic and magnetically ordered states. The spectral functions for the three magnetic states that we have considered are shown in Fig. 4 along with the spectral function for the paramagnetic state. We find that the paramagnetic state is insulating, with a gap only slightly smaller than that of the ground state with [001] antiferromagnetic ordering, indicating that double perovskite Ba_2VFeO_6 is a promising candidate for Mott multiferroics [56]. The calculated spectral functions are

consistent with our schematics of Fig. 3.

We also use our DFT+DMFT methodology to investigate how the electronic structure of Ba_2VFeO_6 evolves as the ferroelectric polarization is suppressed within the paramagnetic state. Fig. 5 compares the spectral function of Ba_2VFeO_6 in the cubic structure (i.e. no polarization) versus in the tetragonal structure (i.e. with polarization). We see that the suppression of polarization reduces the gap by about 0.2 eV. This behavior is very consistent with similar calculations on nonmagnetic perovskite oxide SrTiO_3 in which the presence of ferroelectric polarization can increase the band gap by up to 0.2 eV [60].

E. Hubbard U dependence

Finally we discuss the Hubbard U dependence. As Fig. 4 shows, the conduction band edge is set by V- d states, which is consistent with Fig. 1c and our previous discussion of band gaps. If we change the Hubbard U_V , it may affect the energy position of V d states and energy gap. To address this issue, we repeat the DMFT calculations on tetragonal Ba_2VFeO_6 using several values of U_V . The panels **a** of Fig. 6 show the spectral function of the double perovskite as a function of U_V . All the calculations are performed in a paramagnetic state. We note that as U_V increases from 4 eV to 6 eV, the band gap is almost unchanged. This is due to the fully localized limit double counting correction which nearly cancels the Hartree shift. Hence, the V- d and O- p energy separation is practically unaffected, which is very consistent with the previous DMFT study on SrVO_3 [61]. If we apply the same method and same Hubbard U parameters to tetragonal BaTiO_3 , the spectral functions of BaTiO_3 (panels **b** of Fig. 6) show that the energy gap of BaTiO_3 is slightly increased. Thus while we have some uncertainty relating to the appropriate values for the Hubbard U , our estimates for energy gap are robust: double perovskite Ba_2VFeO_6 has an energy gap ~ 1 eV smaller than that of BaTiO_3 . The underlying reason is the differing electronegativities of Ti^{4+} and V^{5+} .

IV. RELATED MATERIALS Pb_2VFeO_6 AND Sr_2VFeO_6

In this section we employ the same parameters and methods used for Ba_2VFeO_6 to discuss double perovskite Pb_2VFeO_6 and Sr_2VFeO_6 .

We first discuss Pb_2VFeO_6 . Pb has a lone pair of 6s electrons, which favors off-center displacements as was already shown for tetragonal PbTiO_3 [62]. Due to the same mechanism, double perovskite Pb_2VFeO_6 has substantial cation-displacements, tetragonality and ferroelectric polarization (see Table II). All these values are comparable to, or even larger than those of tetragonal PbTiO_3 . We note however that within sPBEsol the polarization of this tetragonal structure is not-well defined because the corresponding high-symmetry cubic structure is metallic and thus the obvious switching path is not available.

While tetragonal double perovskite Pb_2VFeO_6 have similar structural properties to tetragonal PbTiO_3 , the fundamental gap Δ_0 and optical gap Δ_{optical} are both smaller than those of PbTiO_3 by about 1 eV (all three exchange correlation functionals make qualitatively consistent predictions).

We note here that the polarization in Pb_2VFeO_6 has different origin from the polarization in tetragonal PbVO_3 [63]. In tetragonal PbVO_3 , V atoms have a d^1 charge configuration and its off-center displacement δ_{VO} and insulating properties are associated with orbital ordering ($d_{xy}^1 d_{xz}^0 d_{yz}^0$) [64]. In double perovskite oxide Pb_2VFeO_6 , charge transfer leads to a d^0 configuration on V sites and therefore the off-center displacement δ_{VO} is due to hybridization between V- d and O- p states [31]. More importantly, perovskite PbVO_3 is not ferroelectric because along the switching path (from the tetragonal-to-cubic structure) an insulator-to-metal phase transition is observed [65].

Next we discuss Sr_2VFeO_6 . Sr_2VFeO_6 is more complicated because the ionic size of Sr^{2+} is smaller than Ba^{2+} and therefore rotations of oxygen octahedra (so-called antiferrodistortive mode, or AFD mode) can exist in Sr-compounds, such as in SrTiO_3 , which competes against ferroelectric polarization [66]. For double perovskite Sr_2VFeO_6 , even if we do not take the AFD mode into account, different exchange correlation functionals predict different structural and electronic properties. Table III shows that PBE+ U + J predicts that the ground state is tetragonal and ferroelectric. The polarization is sizable ($26 \mu\text{C}/\text{cm}^2$) and the DFT-calculated optical gap is 1.36 eV. On the other hand, the LDA+ U + J method can not stabilize the tetragonal structure. This method predicts that ground state of Sr_2VFeO_6 has a cubic structure with no off-center displacements of either V or Fe, and is metallic. The sPBEsol method can stabilize a tetragonal structure with non-zero off-center displacements δ_{VO} and δ_{FeO} , but the ground state is also metallic and therefore the polarization is not well-defined. We may impose epitaxial strain to induce ferroelectricity in Sr_2VFeO_6 , but

the critical strain strongly depends on the choice of exchange correlation functional [30]: PBE+ $U+J$ does not require any strain to stabilize the ferroelectric state, while LDA+ $U+J$ requires a 3% compressive strain to open the gap and stabilize the tetragonal structure with a sizable polarization. A similar situation occurs for SrTiO₃. If we use the same methods and do not take into account the AFD mode, PBE predicts a ferroelectric ground state, while LDA and sPBE predict that the ground state is cubic (i.e. no polarization). Experimentally, SrTiO₃ is on the verge of a paraelectric-to-ferroelectric transition [67]. Thus we conclude that our DFT calculations indicate that double perovskite Sr₂VFeO₆ is close to the paraelectric-to-ferroelectric phase boundary and probably is on the paraelectric side.

V. CONCLUSIONS

In summary, we use first-principles calculations to design a new class of Mott multiferroics among which double perovskite oxide Ba₂VFeO₆ stands out as a promising candidate to induce bulk photovoltaic effects because of its large polarization (comparable to BaTiO₃); its reduced optical gap (smaller than BaTiO₃ by about 1 eV); and its environmentally friendly composition (Pb-free). Our work shows that charge transfer is a powerful approach to engineering atomic, electronic and magnetic structures in complex oxides. New charge configurations not found in bulk materials can occur in oxide heterostructures (including complex bulk forms such as double perovskites), and these charge configurations can produce emergent phenomena and properties not exhibited in constituent compounds. In particular, V⁵⁺ is very rare in single perovskite oxides (probably due to its small ionic size). We hope our theoretical predictions can stimulate further experimental endeavors to synthesize and measure these new multiferroic materials for photovoltaic applications.

Acknowledgments

H. Chen is supported by National Science Foundation under grant No. DMR-1120296. A. J. Millis is supported by National Science Foundation under grant No. DMR-1308236. Computational facilities are provided via Extreme Science and Engineering Discovery Environment (XSEDE), through Award No. TGPHY130003 and via the National Energy Research Scientific Computing Center (NERSC).

Author Contributions

H. Chen conceived the project and performed numerical calculations. A.J.M supervised the project. H. Chen and A.J.M analyzed the data, discussed the results and wrote the manuscript.

Additional Information

Competing Interests: The authors declare that they have no competing interests.

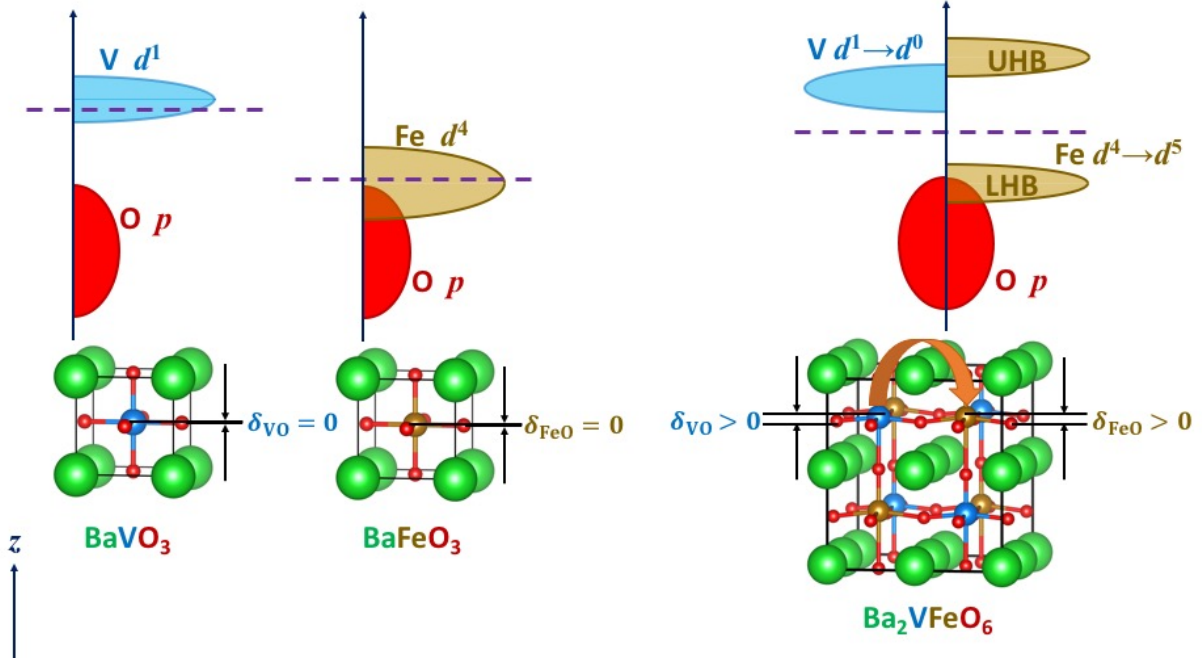


FIG. 1: **Design principles for charge-transfer-driven Mott multiferroics.** a) Energy diagram and atomic structure of cubic BaVO_3 . The dashed line is the Fermi level. δ_{VO} is the V-O displacement along the $[001]$ direction. b) Energy diagram and atomic structure of cubic BaFeO_3 . The dashed line is the Fermi level. δ_{FeO} is the Fe-O displacement along the $[001]$ direction. c) Energy diagram and atomic structure of double perovskite Ba_2VFeO_6 . The dashed line is the Fermi level, which lies in the gap between V d and Fe d states. ‘LHB’ (‘UHB’) means lower Hubbard bands (upper Hubbard bands). The red arrow indicates the charge transfer from V atoms to Fe atoms due to electronegativity difference. In the double perovskite Ba_2VFeO_6 , a polar distortion is developed ($\delta_{\text{VO}} > 0$ and $\delta_{\text{FeO}} > 0$) because of the new charge configuration V d^0 and Fe d^5 .

TABLE I: **Comparison of Ba₂VFeO₆ and BaTiO₃.** The results are calculated using the DFT method with different exchange correlation functionals (xc). ‘nm’ stands for non-magnetic and ‘[001]’ for [001] antiferromagnetic ordering. For the cubic case, a is the lattice constant and Δ_0 is the fundamental gap. For the tetragonal case, a is the in-plane lattice constant, c/a is the ratio of out-of-plane lattice constant over in-plane lattice constant, δ_{BO} is the B -site metal and oxygen displacement along the [001] direction. Δ_0 is the fundamental gap and Δ_{optical} is the optical gap. ΔE is the energy difference between the tetragonal structure and the cubic structure in the unit of meV per 5-atom formula. P is the polarization along the [001] direction. m is the local magnetic moment on V and Fe sites.

	Ba ₂ VFeO ₆			BaTiO ₃		
xc	PBE+ $U+J$	LDA+ $U+J$	sPBEsol	PBE	LDA	sPBEsol
magnetic	[001]	[001]	[001]	nm	nm	nm
	cubic structure					
a (Å)	4.016	3.922	3.965	4.036	3.952	3.991
Δ_0 (eV)	0.55	0.35	0.45	1.70	1.70	1.80
	tetragonal structure					
a (Å)	3.958	3.916	3.946	4.001	3.944	3.978
c/a	1.078	1.007	1.024	1.053	1.011	1.021
δ_{BO} (Å)	0.195 (V) 0.265 (Fe)	0.067 (V) 0.086 (Fe)	0.116 (V) 0.152 (Fe)	0.197	0.099	0.133
P ($\mu\text{C}/\text{cm}^2$)	50	18	34	46	23	33
Δ_0 (eV)	0.78	0.38	0.59	1.75	1.75	1.75
Δ_{optical} (eV)	1.10	1.04	1.17	2.30	2.02	2.14
ΔE (meV)	-43	-1	-7	-56	-6	-17
m (μ_B)	0.129 (V) 4.023 (Fe)	0.071 (V) 4.075 (Fe)	0.091 (V) 4.063 (Fe)	–	–	–

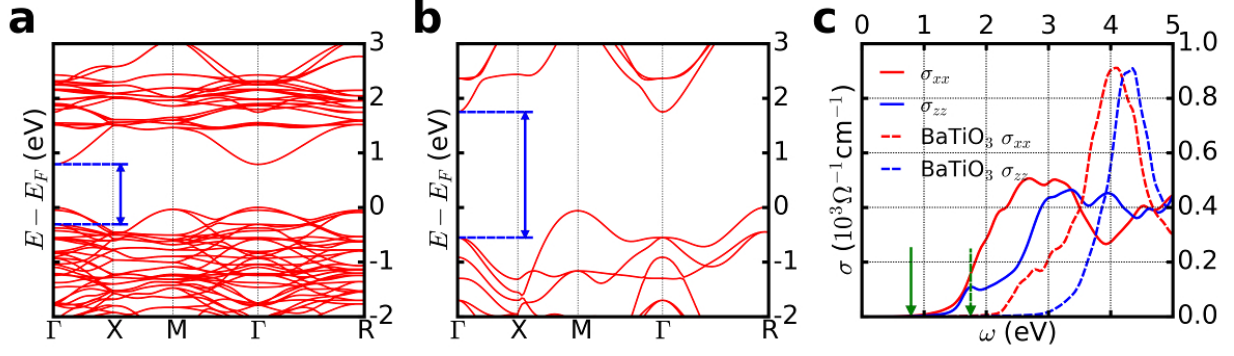


FIG. 2: **Comparison of band structure and optical conductivity between Ba_2VFeO_6 and BaTiO_3 .** The results for Ba_2VFeO_6 are calculated using DFT-PBE+ U + J method. The results for BaTiO_3 are calculated using DFT-PBE method. **a)** Band structure of tetragonal Ba_2VFeO_6 . The blue arrow indicates the threshold of optical transition. **b)** Band structure of tetragonal BaTiO_3 . The blue arrow indicates the threshold of optical transition. **c)** Optical conductivity σ of tetragonal Ba_2VFeO_6 (solid lines) and tetragonal BaTiO_3 (dashed lines). The red lines are for the xx -component and the blue lines are for the zz -component. The green arrows indicate the fundamental gap of band structures.

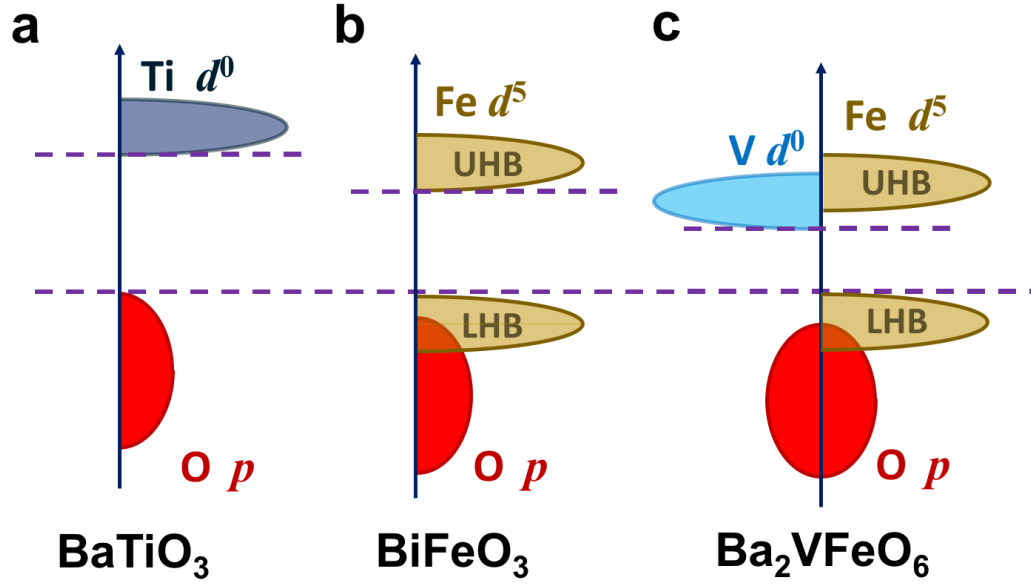


FIG. 3: Comparison of gaps for different perovskite oxides. a) BaTiO₃; b) BiFeO₃; c) Ba₂VFeO₆. ‘LHB’ (‘UHB’) means lower Hubbard bands (upper Hubbard bands). The valence band edges are aligned for comparison.

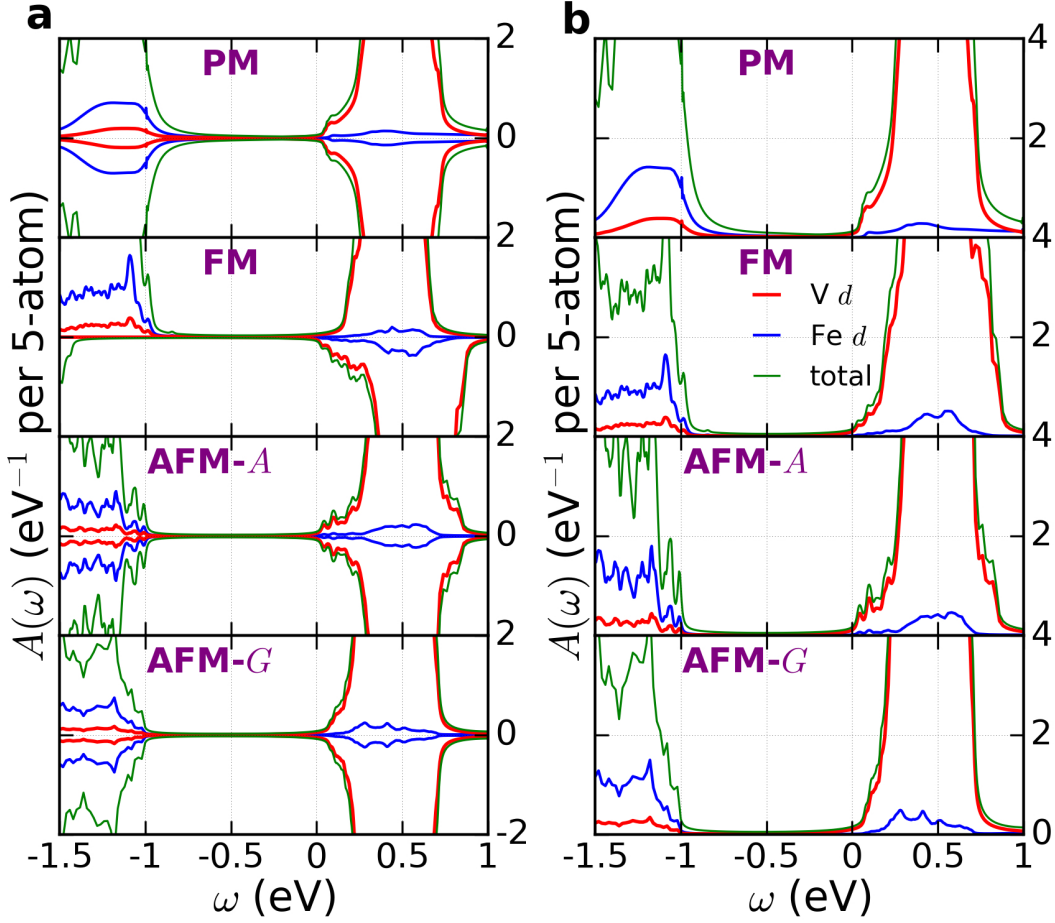


FIG. 4: Spectral functions $A(\omega)$ of tetragonal double perovskite Ba_2VFeO_6 for different magnetic states. The unit of $A(\omega)$ is eV^{-1} per 5-atom. ‘PM’ stands for paramagnetic state, ‘FM’ for ferromagnetic state, ‘[001]-AFM’ for [001] antiferromagnetic state and ‘[100]-AFM’ for [100] antiferromagnetic state. Panels a) spin-resolved spectral function. The positive (negative) y -axis corresponds to spin-up (spin-down). Panels b) total spectral functions (summing over spin-up and spin-down). The red, blue and green curves are for Fe d , V d and O p , respectively. The Fermi level is set at $\omega = 0$ eV.

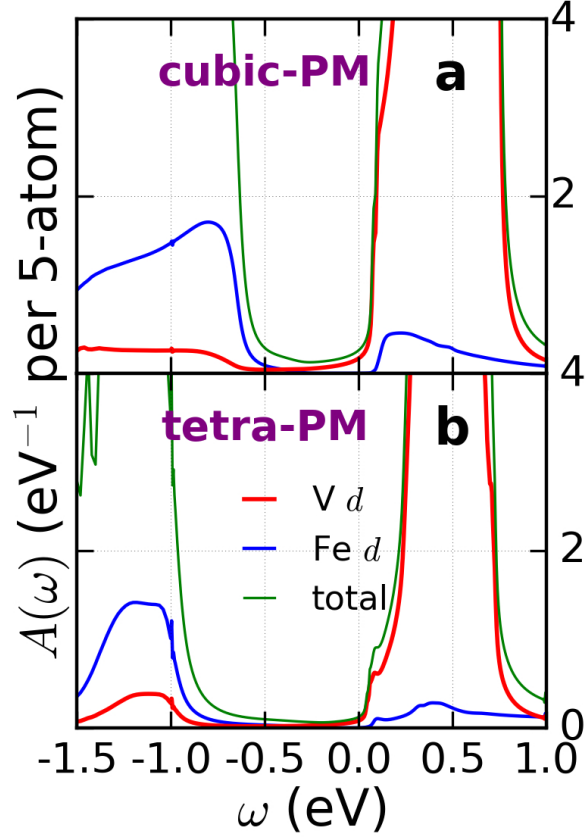


FIG. 5: **Spectral functions $A(\omega)$ of cubic and tetragonal Ba_2VFeO_6 .** The unit of $A(\omega)$ is eV^{-1} per 5-atom. Panel **a** is for cubic Ba_2VFeO_6 and panel **b** is for tetragonal Ba_2VFeO_6 . In both structures, we calculate the paramagnetic state. The red, blue and green curves are for Fe d , V d and O p , respectively. The Fermi level is set at $\omega = 0$ eV.

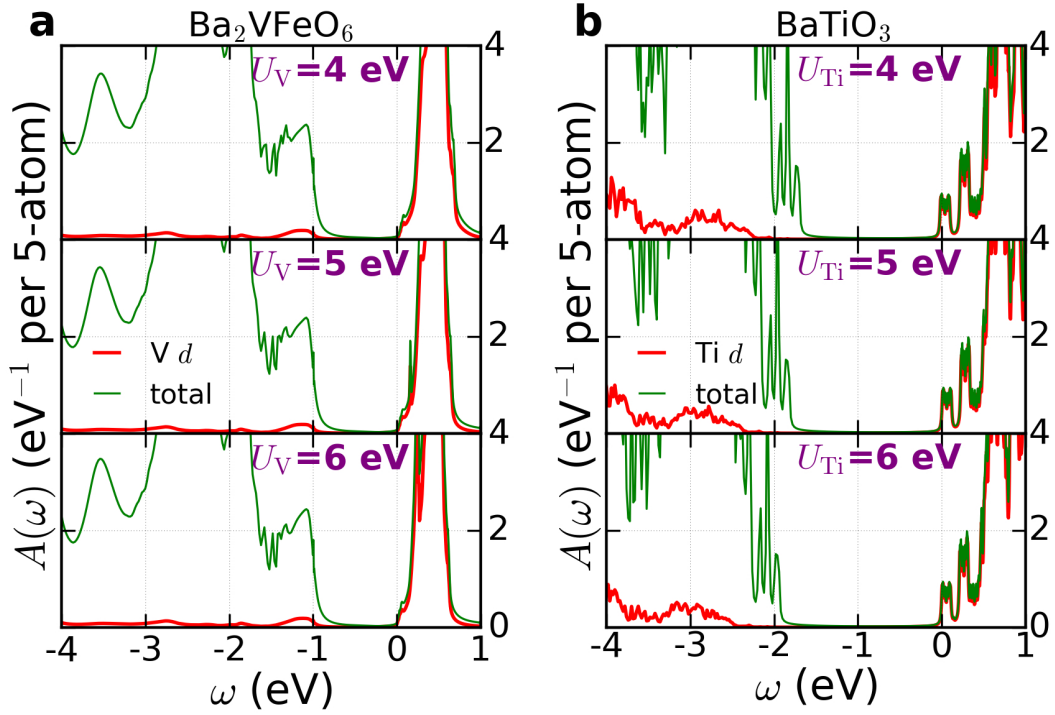


FIG. 6: Spectral functions $A(\omega)$ of tetragonal Ba_2VFeO_6 and BaTiO_3 as a function of Hubbard U on V and Ti. The unit of $A(\omega)$ is eV^{-1} per 5-atom. Panels **a** are the results for tetragonal Ba_2VFeO_6 . Panels **b** are the results for tetragonal BaTiO_3 . For Ba_2VFeO_6 , the calculations are performed in a paramagnetic state. For BaTiO_3 , the calculations are performed in a non-magnetic state. In panels **a**, the green lines are the total spectral functions and the red lines are the spectral functions projected onto V d states. In panels **b**, the green lines are the total spectral functions and the red lines are the spectral functions projected onto Ti d states. The Fermi level is set at $\omega = 0$ eV.

TABLE II: **Comparison of Pb_2VFeO_6 and PbTiO_3 .** The results are calculated using the DFT method with different exchange correlation functionals (xc). ‘nm’ stands for non-magnetic and ‘[001]’ for the [001] antiferromagnetic ordering. For the cubic case, a is the lattice constant and Δ_0 is the fundamental gap. For the tetragonal case, a is the in-plane lattice constant, c/a is the ratio of out-of-plane lattice constant over in-plane lattice constant, δ_{BO} is the B -site metal and oxygen displacement along the [001] direction. Δ_0 is the fundamental gap and Δ_{optical} is the optical gap. ΔE is the energy difference between the tetragonal structure and the cubic structure in the unit of meV per 5-atom formula. P is the polarization along the [001] direction. m is the local magnetic moment on V and Fe sites.

	Pb_2VFeO_6			PbTiO_3		
xc	PBE+ $U+J$	LDA+ $U+J$	sPBEsol	PBE	LDA	PBEsol
magnetic	[001]	[001]	[001]	nm	nm	nm
	cubic structure					
a (Å)	3.949	3.857	3.887	3.972	3.891	3.929
Δ_0 (eV)	0.60	0.41	metallic	1.61	1.47	1.53
	tetragonal structure					
a (Å)	3.803	3.776	3.751	3.844	3.865	3.882
c/a	1.248	1.116	1.220	1.238	1.044	1.081
δ_{BO} (Å)	0.425 (V) 0.629 (Fe)	0.281 (V) 0.463 (Fe)	0.413 (V) 0.601 (Fe)	0.526	0.277	0.346
P ($\mu\text{C}/\text{cm}^2$)	124	102	–	125	79	93
Δ_0 (eV)	0.42	0.38	0.26	1.88	1.49	1.60
Δ_{optical} (eV)	1.83	1.83	1.88	2.86	2.48	2.82
ΔE (meV)	-251	-77	-239	-209	-57	-79
m (μ_B)	0.147 (V) 4.004 (Fe)	0.163 (V) 4.002 (Fe)	0.183 (V) 3.674 (Fe)	–	–	–

TABLE III: **Comparison of Sr_2VFeO_6 and SrTiO_3 .** The results are calculated using the DFT method with different exchange correlation functionals (xc). Antiferrodistortive modes are not taken into account in the calculations. ‘nm’ stands for non-magnetic and ‘[001]’ for the [001] antiferromagnetic ordering. For the cubic case, a is the lattice constant and Δ_0 is the fundamental gap. For the tetragonal case, a is the in-plane lattice constant, c/a is the ratio of out-of-plane lattice constant over in-plane lattice constant, δ_{BO} is the B -site metal and oxygen displacement along the [001] direction. Δ_0 is the fundamental gap and Δ_{optical} is the optical gap. ΔE is the energy difference between the tetragonal structure and the cubic structure in the unit of meV per 5-atom formula. P is the polarization along the [001] direction. m is the local magnetic moment on V and Fe sites.

	Sr_2VFeO_6			SrTiO_3		
xc	PBE+ $U+J$	LDA+ $U+J$	sPBEsol	PBE	LDA	PBEsol
magnetic	[001]	[001]	[001]	nm	nm	nm
	cubic structure					
a (Å)	3.915	3.823	3.853	3.944	3.863	3.903
Δ_0 (eV)	0.40	metallic	metallic	1.79	1.80	1.81
	tetragonal structure					
a (Å)	3.904	–	3.841	3.936	–	–
c/a	1.013	–	1.017	1.011	–	–
δ_{BO} (Å)	0.109 (V) 0.120 (Fe)	–	0.181 (V) 0.162 (Fe)	0.120	–	–
P ($\mu\text{C}/\text{cm}^2$)	26	–	metallic	30	–	–
Δ_0 (eV)	0.30	–	metallic	1.82	–	–
Δ_{optical} (eV)	1.36	–	metallic	2.34	–	–
ΔE (meV)	-2	0	-34	-6	0	0
m (μ_B)	0.084 (V) 4.089 (Fe)	0.061 (V) 4.107 (Fe)	0.113 (V) 3.543 (Fe)	–	–	–

-
- [1] S. Y. Yang, Nat. Nanotechnol. **5**, 143 (2010).
 - [2] D. Cao, C. Wang, F. Zheng, W. Dong, L. Fang, and M. Shen, Nano Lett. **12**, 2803 (2012).
 - [3] M. Alexe, Nat. Commun. **2**, 256 (2011).
 - [4] I. Grinberg, D. V. West, M. Torres, G. Gou, D. M. Stein, L. Wu, G. Chen, E. M. Gallo, A. R. Akbashev, P. K. Davies, et al., Nature **503**, 509 (2013).
 - [5] D. I. Bilc, R. Orlando, R. Shaltaf, G. M. Rignanes, J. Íñiguez, and P. Ghosez, Phys. Rev. B **77** (2008).
 - [6] J. W. Bennett, I. Grinberg, and A. M. Rappe, J. Am. Chem. Soc. **130**, 17409 (2008).
 - [7] G. Y. Gou, J. W. Bennett, H. Takenaka, and A. M. Rappe, Phys. Rev. B **83** (2011).
 - [8] T. Qi, I. Grinberg, and A. M. Rappe, Phys. Rev. B **83** (2011).
 - [9] T. Choi, S. Lee, Y. J. Choi, V. Kiryukhin, and S.-W. Cheong, Science **324**, 63 (2009).
 - [10] W. S. Choi, Nat. Commun. **3**, 689 (2012).
 - [11] R. Nechache, C. Harnagea, S. Li, L. Cardenas, W. Huang, J. Chakrabartty, and F. Rosei, Nat. Photonics **61**, 61 (2014).
 - [12] C. Kim, H. Park, and C. A. Marianetti, Phys. Rev. B **92** (2015).
 - [13] H. Chen, D. Kumah, A. Disa, F. Walker, C. Ahn, and S. Ismail-Beigi, Phys. Rev. Lett. **110** (2013).
 - [14] H. Chen, A. Millis, and C. Marianetti, Phys. Rev. Lett. **111**, 116403 (2013).
 - [15] J. E. Kleibecker, Z. Zhong, H. Nishikawa, J. Gabel, A. Müller, F. Pfaff, M. Sing, K. Held, R. Claessen, G. Koster, et al., Phys. Rev. Lett. **113**, 237402 (2014).
 - [16] A. Disa, D. Kumah, A. Malashevich, H. Chen, D. Arena, E. Specht, S. Ismail-Beigi, F. Walker, and C. Ahn, Phys. Rev. Lett. **114**, 026801 (2015).
 - [17] Y. Cao, X. Liu, M. Kareev, D. Choudhury, S. Middey, D. Meyers, J. W. Kim, P. Ryan, J. W. Freeland, and J. Chakhalian, Nat. Commun. **7**, 10418 (2016).
 - [18] M. N. Grisolia, J. Varignon, G. Sanchez-Santolino, A. Arora, S. Valencia, M. Varela, R. Abrandan, E. Weschke, E. Schierle, J. E. Rault, et al., Nat. Phys. **12**, 484 (2016).
 - [19] K. Nishimura, I. Yamada, K. Oka, Y. Shimakawa, and M. Azuma, J. Phys. Chem. Solids **75**, 710 (2014).
 - [20] N. Hayashi, T. Yamamoto, H. Kageyama, M. Nishi, Y. Watanabe, T. Kawakami, Y. Mat-

- sushita, A. Fujimori, and M. Takano, *Angew. Chemie - Int. Ed.* **50**, 12547 (2011).
- [21] T. Matsui, H. Tanaka, N. Fujimura, T. Ito, H. Mabuchi, and K. Morii, *Appl. Phys. Lett.* **81**, 2764 (2002).
 - [22] T. Matsui, E. Taketani, N. Fujimura, T. Ito, and K. Morii, *J. Appl. Phys.* **93**, 6993 (2003).
 - [23] C. Callender, D. P. Norton, R. Das, A. F. Hebard, and J. D. Budai, *Appl. Phys. Lett.* **92**, 012514 (2008).
 - [24] S. Chakraverty, T. Matsuda, N. Ogawa, H. Wadati, E. Ikenaga, M. Kawasaki, Y. Tokura, and H. Y. Hwang, *Appl. Phys. Lett.* **103** (2013).
 - [25] H. Chen and A. Millis, *Phys. Rev. B* **93**, 104111 (2016).
 - [26] H. W. Eng, P. W. Barnes, B. M. Auer, and P. M. Woodward, in *J. Solid State Chem.* (2003), vol. 175, pp. 94–109.
 - [27] R. F. Berger and J. B. Neaton, *Phys. Rev. B* **86**, 165211 (2012).
 - [28] J. B. Neaton, C. Ederer, U. V. Waghmare, N. A. Spaldin, and K. M. Rabe, *Phys. Rev. B* **71**, 014113 (2005).
 - [29] J. M. Rondinelli, A. S. Eidelson, and N. A. Spaldin, *Phys. Rev. B* **79**, 205119 (2009).
 - [30] H. Chen and A. J. Millis, *Phys. Rev. B* **93**, 045133 (2016).
 - [31] N. A. Benedek and T. Birol, *Mater. Chem. C* **4**, 4000 (2016).
 - [32] M. C. Knapp and P. M. Woodward, *J. Solid State Chem.* **179**, 1076 (2006).
 - [33] M. C. Payne, M. P. Teter, D. C. Allan, T. A. Arias, and J. D. Joannopoulos, *Rev. Mod. Phys.* **64**, 1045 (1992).
 - [34] G. Kotliar, S. Savrasov, K. Haule, V. Oudovenko, O. Parcollet, and C. Marianetti, *Rev. Mod. Phys.* **78**, 865 (2006).
 - [35] H. Chen and A. Millis, *Phys. Rev. B* **93**, 205110 (2016).
 - [36] J. P. Perdew, K. Burke, and M. Ernzerhof, *Phys. Rev. Lett.* **77**, 3865 (1996).
 - [37] A. I. Liechtenstein, V. I. Anisimov, and J. Zaanen, *Phys. Rev. B* **52**, R5467 (1995).
 - [38] W. Kohn and L. J. Sham, *Phys. Rev.* **140**, A1133 (1965).
 - [39] J. P. Perdew, A. Ruzsinszky, G. I. Csonka, O. A. Vydrov, G. E. Scuseria, L. A. Constantin, X. Zhou, and K. Burke, *Phys. Rev. Lett.* **100**, 136406 (2008).
 - [40] G. Kresse and J. Furthmüller, *Comput. Mater. Sci.* **6**, 15 (1996).
 - [41] G. Kresse and J. Furthmüller, *Phys. Rev. B* **54**, 11169 (1996).
 - [42] P. E. Blöchl, *Phys. Rev. B* **50**, 17953 (1994).

- [43] G. Kresse, Phys. Rev. B **59**, 1758 (1999).
- [44] E. Pavarini, S. Biermann, A. Poteryaev, A. I. Lichtenstein, A. Georges, and O. K. Andersen, Phys. Rev. Lett. **92**, 176403 (2004).
- [45] N. J. Mosey, P. Liao, and E. A. Carter, J. Chem. Phys. **129**, 014103 (2008).
- [46] P. Werner, A. Comanac, L. De' Medici, M. Troyer, and A. J. Millis, Phys. Rev. Lett. **97**, 076405 (2006).
- [47] E. Gull, A. J. Millis, A. I. Lichtenstein, A. N. Rubtsov, M. Troyer, and P. Werner, Rev. Mod. Phys. **83**, 349 (2011).
- [48] N. Marzari, A. A. Mostofi, J. R. Yates, I. Souza, and D. Vanderbilt, Rev. Mod. Phys. **84**, 1419 (2012).
- [49] R. N. Silver, D. S. Sivia, and J. E. Gubernatis, Phys. Rev. B **41**, 2380 (1990).
- [50] M. T. Czyżyk and G. A. Sawatzky, Phys. Rev. B **49**, 14211 (1994).
- [51] X. Wu, K. M. Rabe, and D. Vanderbilt, Phys. Rev. B **83**, 020104 (2011).
- [52] H. Chen, A. J. Millis, and C. A. Marianetti, Phys. Rev. Lett. **111**, 116403 (2013).
- [53] M. Gajdoš, K. Hummer, G. Kresse, J. Furthmüller, and F. Bechstedt, Phys. Rev. B **73**, 045112 (2006).
- [54] J. F. Ihlefeld, N. J. Podraza, Z. K. Liu, R. C. Rai, X. Xu, T. Heeg, Y. B. Chen, J. Li, R. W. Collins, J. L. Musfeldt, et al., Appl. Phys. Lett. **92**, 142908 (2008).
- [55] D. Khomskii, Physics (College. Park. Md). **2**, 20 (2009).
- [56] D. Puggioni, G. Giovannetti, M. Capone, and J. M. Rondinelli, Phys. Rev. Lett. **115**, 087202 (2015).
- [57] S. C. Abrahams, S. K. Kurtz, and P. B. Jamieson, Phys. Rev. **172**, 551 (1968).
- [58] I. Grinberg and A. M. Rappe, Phys. Rev. B **70**, 220101 (2004).
- [59] H. D. Megaw, Proc. Phys. Soc. **58**, 133 (1946).
- [60] R. F. Berger, C. J. Fennie, and J. B. Neaton, Phys. Rev. Lett. **107**, 146804 (2011).
- [61] H. T. Dang, A. J. Millis, and C. A. Marianetti, Phys. Rev. B **89**, 161113 (2014).
- [62] U. V. Waghmare and K. M. Rabe, Phys. Rev. B **55**, 6161 (1997).
- [63] R. V. Shpanchenko, V. V. Chernaya, A. A. Tsirlin, P. S. Chizhov, D. E. Sklovsky, E. V. Antipov, E. P. Khlybov, V. Pomjakushin, A. M. Balagurov, J. E. Medvedeva, et al., Chem. Mater. **16**, 3267 (2004).
- [64] K. Oka, I. Yamada, M. Azuma, S. Takeshita, K. H. Satoh, A. Koda, R. Kadono, M. Takano,

- and Y. Shimakawa, *Inorg. Chem.* **47**, 7355 (2008).
- [65] A. A. Belik, M. Azuma, T. Saito, Y. Shimakawa, and M. Takano, *Chem. Mater.* **17**, 269 (2005).
- [66] P. A. Fleury, J. F. Scott, and J. M. Worlock, *Phys. Rev. Lett.* **21**, 16 (1968).
- [67] K. A. Müller and H. Burkard, *Phys. Rev. B* **19**, 3593 (1979).